

# Effect of reaction temperature on surface morphology and photoelectric properties of ZnO grown by hydrothermal method in mixed solvent

Jianguo Lv<sup>1</sup> · Yue Sun<sup>1</sup> · Li Cao<sup>1</sup> · Min Zhao<sup>1</sup> · Fengjiao Shang<sup>1</sup> · Sicong Mao<sup>1</sup> · Yaoyao Jiang<sup>1</sup> · Jinhua Xu<sup>1</sup> · Feng Wang<sup>1</sup> · Zhitao Zhou<sup>1</sup> · Yiyong Wei<sup>1</sup> · Gang He<sup>2</sup> · Miao Zhang<sup>2</sup> · Xueping Song<sup>2</sup> · Zhaoqi Sun<sup>2</sup>

Received: 3 February 2015 / Accepted: 21 April 2015 / Published online: 1 May 2015  
© Springer Science+Business Media New York 2015

**Abstract** ZnO thin films were prepared by hydrothermal method in mixed solvent with different reaction temperatures. Microstructure, surface morphology, optical properties and UV photoresponse of the thin films have been investigated by means of X-ray diffractometer, scanning electron microscopy, laser micro-Raman spectrometer, UV–Vis spectrophotometer and interactive source meter instrument. The results indicated that ZnO thin films consist of ZnO nanoparticles with hexagonal wurzite structure. A small quantity of Zn(OH)<sub>2</sub> appear as reaction temperature increase to 125 °C. ZnO thin film grown at 175 °C consists of many densely vertically aligned ZnO nano rods on the substrate and has the best preferential *c*-axis orientation. Three peaks centered at about 446, 568 and 1150 cm<sup>-1</sup> have been attributed to *E*<sub>2</sub>(high), *A*<sub>1</sub>(*LO*) and 2*A*<sub>1</sub>(*LO*) phonon mode. Broadening of the visible emission band may be attributed to abundant surface defects and surface states of the thin films. Variation of the *E*<sub>g</sub> may be attributed to the synergy of surface

morphology and oxygen-vacancy (*V*<sub>O</sub>) density. The fast and slow UV photo response may be attributed to the adsorption and photo desorption of oxygen molecules on the surface of ZnO thin films and exchange process between oxygen gas and native deep defect level, respectively.

## 1 Introduction

ZnO is an important semiconductor material because of its wide direct band gap (3.37 eV) and high exciton binding energy (60 meV) at room temperature, as well as low-cost manufacturing and environmentally friendly. It makes ZnO as a promising photoelectric material for applications such as field-emission devices [1], solar cells [2], nanosensors [3], light-emitting diodes (LEDs) [4], laser diodes (LDs) [5] and UV photodetectors [6]. It has been reported that ZnO nano structure thin films show much more enhanced photoelectric properties than the ZnO bulk due to the surface effect and size effect. ZnO nanostructure thin films have been synthesized by RF magnetron sputtering [7], metal organic chemical vapor deposition (MOCVD) [8], pulsed laser deposition (PLD) [9], sol–gel method [10] and hydrothermal method [11]. Among the above methods, hydrothermal method is a preferred method because of its many advantages like low energy consumption, cost-effectiveness, simple equipment requirement and mild reaction condition.

In the present paper, the mixed solvents of water and ethylene glycol monomethyl ether were selected in hydrothermal process. Effects of reaction temperature on microstructure, surface morphology and optical properties of ZnO thin films have been investigated. Photoresponse of the thin film to UV light has been measured and formation mechanism has been studied in detail.

---

✉ Min Zhao  
zhaomin@hftc.edu.cn

✉ Gang He  
hegang@ahu.edu.cn

✉ Zhaoqi Sun  
szq@ahu.edu.cn

<sup>1</sup> School of Electronic and Information Engineering, Hefei Normal University, Hefei 230601, China

<sup>2</sup> School of Physics and Material Science, Anhui University, Hefei 230039, China

## 2 Experimental

### 2.1 Synthesis of ZnO thin films

The cleaned silicon substrates were used for the deposition of ZnO seed layers by sol–gel method. In brief, 8.76 g zinc acetate dehydrate  $[\text{Zn}(\text{CH}_3\text{COO})_2 \cdot 2\text{H}_2\text{O}]$  was dissolved into 80 mL ethylene glycol monomethyl ether at room temperature. Equimolar monoethanol amine (MEA) was added to the solution as a stabilizing agent. The solution was stirred at 60 °C for 120 min to get a homogeneous and transparent sol, which served as the coating sol after being kept for 24 h. ZnO seed layers were deposited on silicon substrates by spin coating with 3000 rpm for 30 s. After each spin coating, the silicon substrates were put into an oven at 150 °C for 10 min to evaporate the solvent and remove organic residuals. This procedure was repeated two times. Finally, the seed layers were inserted to a furnace and annealed at the temperature of 600 °C for 240 min. The obtained ZnO seed layer on silicon substrates was used for the deposition of ZnO thin films. The ZnO thin films were grown by the hydrothermal method using ZnO seed layer as substrate. Typically, zinc nitrate hexahydrate  $(\text{Zn}(\text{NO}_3)_2 \cdot 6\text{H}_2\text{O})$  and equimolar hexamethylenetetramine  $(\text{C}_6\text{H}_{12}\text{N}_4, \text{HMT})$  dissolved in 40 mL mixed solvents of water and ethylene glycol monomethyl ether. The ratio of water and ethylene glycol monomethyl ether in the mixed solvents were 0.25. The concentration of zinc nitrate hexahydrate was 0.06 mol/L. Subsequently, the solution was transferred to a 50 mL Teflon-lined stainless steel autoclave and the ZnO seed layers were placed upside down in the bottom of the autoclave. Growth of ZnO thin films were performed at 95, 105, 125, 175 °C for 2 h in an oven. The ZnO thin films were removed from the solutions and rinsed several times with deionized water, and then dried at 60 °C in air.

### 2.2 Characterization

Microstructures of ZnO thin films were investigated by a X-ray diffractometer (XRD, TD3500) with  $\text{CuK}\alpha$  radiation ( $\lambda = 0.15405 \text{ nm}$ ) and operated at 40 kV and 30 mA from 30° to 80°. Surface morphologies of the thin films were observed by scanning electron microscopy (SEM, HITACHI SU1510). Photoluminescence (PL) spectra and Raman spectra of the thin films were performed by a laser micro-Raman spectrometer (Renishaw in Via-Reflex) using He–Cd laser as light source excited at 325 nm. PL spectra were examined in the wavelength range of 340–640 nm. Raman spectra were recorded in the range of 100–1600  $\text{cm}^{-1}$ . Absorption spectra of the thin films were tested by UV–Vis spectrophotometer (UV–Vis, SHIMADZU UV 2550).

Absorption spectra were recorded in the wavelength range of 300–900 nm. The photocurrent responses of the thin films were measured by an interactive source meter instrument (Keithley 2450) at a fixed bias of 5 V by switching the UV light ( $\lambda = 254 \text{ nm}$ ) with a power intensity of 15  $\mu\text{W}/\text{cm}^2$ .

## 3 Results and discussion

Typical XRD patterns of ZnO thin films are shown in Fig. 1. It can be seen that seven diffraction peaks appear at  $2\theta = 31.77^\circ, 34.42^\circ, 36.25^\circ, 47.54^\circ, 62.86^\circ, 67.96^\circ$  and  $69.10^\circ$  corresponding to (100), (002), (101), (102), (103), (112) and (201) planes of wurzite ZnO (JCPDS 36–1451), respectively. One diffraction peak appear at  $2\theta = 31.10^\circ$  corresponding to (080) planes of  $\text{Zn}(\text{OH})_2$  (JCPDS 20–1437), which grows at the temperature of 125 and 175 °C. As reaction temperature increases from 95 to 175 °C, the relative intensity of the (002) diffraction peak in one XRD pattern decreases first and then increases. In order to characterize quantitatively the preferential orientation of the thin films, the texture coefficient  $\text{TC}_{(hkl)}$  has been calculated by using the following relation [12]:

$$\text{TC}_{(hkl)} = \frac{I_{(hkl)}/I_{0(hkl)}}{\frac{1}{N} \sum_N I_{(hkl)}/I_{0(hkl)}} \quad (1)$$

where  $I_{(hkl)}$  is the measured relative intensity of the (hkl) plane,  $I_{0(hkl)}$  is the standard relative intensity of the (hkl) plane taken from the JCPDS 36–1451 data, and  $N$  is the total number of reflection peaks from the thin film. In the present letter,  $n = 4$  because four major reflection peaks come from (100), (002), (101), and (103) planes are involved. The value,  $\text{TC}_{(hkl)} = 1$ , represents the thin film with randomly oriented crystallites, while higher value indicates the abundance of crystallites oriented along (hkl) direction.  $\text{TC}_{(hkl)}$  of ZnO thin films are listed in Table 1. It

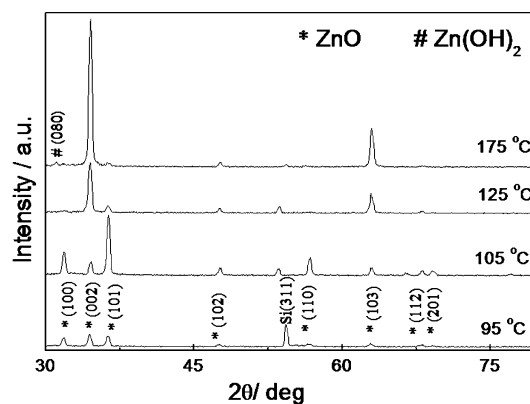
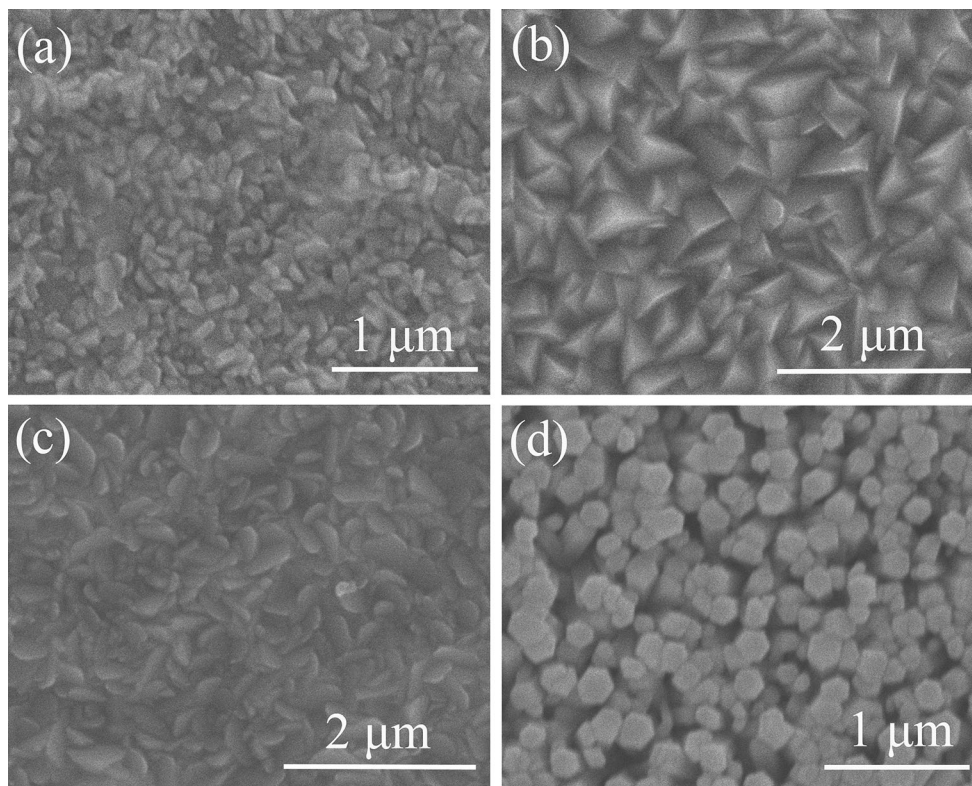


Fig. 1 XRD patterns of ZnO thin films

**Table 1** Texture coefficient and optical band gap of ZnO thin films

Reaction temperature (°C)	Texture coefficient ( <i>TC</i> )				$E_g/eV$
	$TC_{(100)}$	$TC_{(002)}$	$TC_{(101)}$	$TC_{(103)}$	
95	0.93	1.63	0.62	0.82	3.221
105	1.06	0.78	1.44	0.72	3.181
125	0.13	2.39	0.17	1.31	2.211
175	0.06	2.79	0.05	1.10	3.179

**Fig. 2** SEM images of ZnO thin films with different reaction temperature. **a** 95 °C, **b** 105 °C, **c** 125 °C and **d** 175 °C

can be seen from Table 1 that the value of  $TC_{(002)}$  decreases to a minimum at 105 °C and then increases with the increase of reaction temperature. The results tell us that the ZnO thin films grown at the temperature of 175 °C has the best preferential *c*-axis orientation.

Figure 2 shows the SEM images of ZnO thin films with different reaction temperature. It can be seen that the reaction temperatures have an important influence on surface morphology of the thin films. The ZnO thin film, which grows at the temperature of 95 °C, is composed of a lot of sparse small particles. As reaction temperature increases to 105 °C, the thin film consists of dense and packed pyramidal particles. As the reaction temperature further increases to 125 °C, the surface morphology of the thin film change into nano-sheets. The ZnO thin film, which grows at the temperature of 175 °C, consists of many densely vertically aligned ZnO nanorods on the silicon substrate. This result is identical with the test by XRD.

The saturated vapor pressure is in proportion to the reaction temperature. So, evolution of the surface morphology may be attributed to change of saturated vapor pressure.

In order to provide additional information of the samples, the Raman scattering spectra were used to investigate the vibrational properties of the ZnO thin films at room temperature. Figure 3 presents the Raman scattering spectra of ZnO thin films with  $\lambda = 325$  nm at room temperature. It can be seen that three peaks centered at about 446, 568 and 1150  $\text{cm}^{-1}$  have been observed in all the thin films. ZnO with wurtzite structure belongs to the  $C_{6v}$  space group with the two formula units per primitive cell and all the atoms occupy the  $C_{3v}$  symmetry. The peak centered at about 446  $\text{cm}^{-1}$  is assigned to the  $E_2(\text{high})$  phonon mode [13]. The peak at about 568  $\text{cm}^{-1}$  which is attributed to the  $A_1(\text{LO})$  phonon mode. The peak located at 1150  $\text{cm}^{-1}$  is assigned to the  $2A_1(\text{LO})$  phonon mode [14].

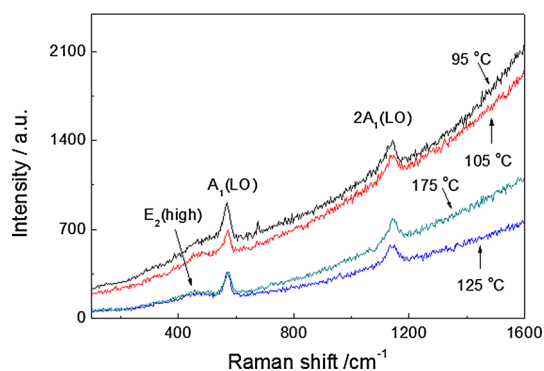


**Fig. 3** Raman spectra of ZnO thin films

Figure 4 shows the room temperature PL spectrum of the ZnO thin film. It can be seen that the PL spectrum consists of a strong and sharp UV emission peak and a weak and broad visible emission band. The UV emission peak at about 378 nm is corresponding to the ZnO thin film. The result is good consistent with the reports of other researchers [15, 16]. Generally, the UV emission is attributed to the radiative recombination of free excitons. Effect of reaction temperature on position of UV emission peak may be attributed to quantum confinement and nanoparticle shape of ZnO thin films [15]. It has been generally accepted that the green emission in the range between 440 and 650 nm is associated with oxygen vacancies [17, 18]. On the other hand, surface states have also been identified as a possible cause of the green emission in ZnO nanostructures [19]. Mahmood et al. [20] have proposed that the surface states in ZnO nanostructures may play an important role in the green emission. Therefore, they thought that both oxygen vacancy and surface states may be responsible for the green emission of ZnO nanostructures. As reaction temperature increases from 95 to 175 °C, broadening of the visible emission band may be attributed to abundant surface defects and surface states of the thin films with the larger specific surface area.

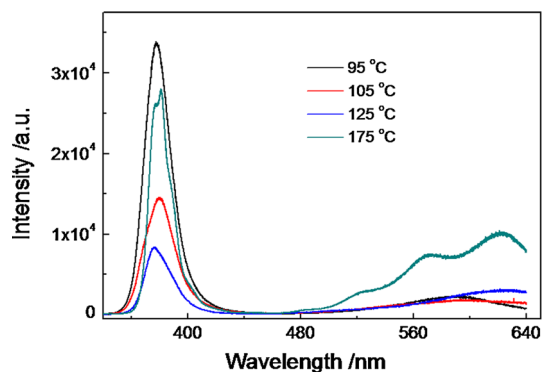


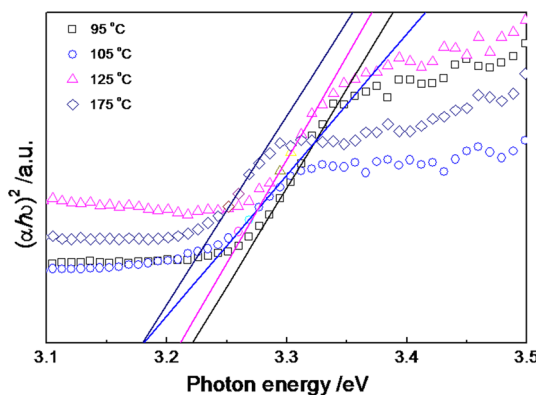
**Fig. 4** Room temperature PL spectra of ZnO thin films

In order to study the relation between optical band gap  $E_g$  and reaction temperature, the absorption spectra of the ZnO thin films have been observed by UV–Vis spectrophotometer. For the direct band gap semiconductor, the optical band gap  $E_g$  can be obtained by using the following equations [21]:

$$\alpha h\nu = A(h\nu - E_g)^{1/2} \tag{2}$$

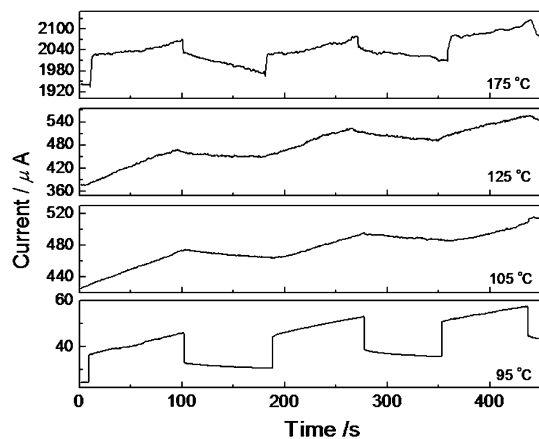
where  $\alpha$  is the optical absorption coefficient,  $A$  is the constant,  $h$  is the Planck’s constant and  $\nu$  is the photon frequency. Plots of  $(\alpha h\nu)^2$  versus  $h\nu$  of the thin films are shown in Fig. 5. The value of  $E_g$  can be obtained by extrapolating the straight linear portion of the plots between  $(\alpha h\nu)^2$  and  $h\nu$  to the phonon energy axis [22]. The optical band gaps of the thin films are shown in Table 1. The maximum and minimum band gaps of 3.221 and 3.179 eV have been observed in the thin films grown at the temperature of 95 and 175 °C, respectively. Generally, change of band gap of ZnO thin film may be due to the variation of surface morphology [23], size effect [24], oxygen-vacancy ( $V_O$ ) density [25], impurity levels [21], and Burstein–Moss shift [26]. In our case, the variation of the  $E_g$  may be attributed to the synergy of surface morphology and oxygen-vacancy ( $V_O$ ) density.

Figure 6 exhibits the time-dependent photoresponse of ZnO thin film illuminated by 254 nm UV light under a bias voltage of 5 V in the atmosphere. It can be seen that the thin films grow at 95 and 175 °C have a fast growth and decay when the UV light is turned on–off. But the thin films grown at 105 and 125 °C exhibit a slow growth and decay when the UV light is turned on–off. The fast UV response may be attributed to the adsorption and photodesorption of oxygen molecules on the surface of ZnO thin films. Before UV irradiation, oxygen molecules are adsorbed onto the surfaces of ZnO thin film by capturing free electrons from the ZnO and forming a low-conductivity depletion layer near the surface [27].

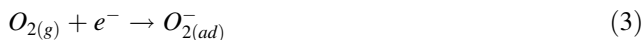


**Fig. 5** Plots of  $(\alpha h\nu)^2$  versus  $h\nu$  of ZnO thin films





**Fig. 6** Photocurrent growth and decay under the periodic illumination of UV light at 5 V bias voltages



When ZnO thin film is illuminated by UV light with photon energies above the band gap of ZnO, UV photon is absorbed by the ZnO and the electron–hole pairs are generated. A portion of holes are drifted by the surface electric field in the depletion layer. The migrated holes can neutralize the surface adsorbed oxygen and resulting in the decrease of depletion layer near the surface [27].



Therefore, enhancement of the conductivity may be due to the increased free carrier concentration and the decreased depletion width near the surface. The photocurrent following a fast growth and decay in the beginning and has a long tail close to the stable value. For the ZnO thin film, growth or decay duration may also partly come from the exchange process between oxygen gas and native deep defect level [28]. This exchange process is much slower than the surface process due to higher activation energy. The slow growth and decay for the thin films grown at 105 and 125 °C may be come mainly from interactions between oxygen gas and native deep defects [29].

## 4 Conclusions

Microstructure, surface morphology and photoelectric properties of the thin films, which were grown by hydrothermal process with different reaction temperatures, were measured by XRD, SEM, laser micro-Raman spectrometer, UV–Vis spectrophotometer and source meter instrument. The best preferential *c*-axis orientation and aligned ZnO nanorods has been observed in the ZnO thin

film grown at the temperature of 175 °C. Three peaks centered at about 446, 568 and 1150  $\text{cm}^{-1}$  have been attributed to  $E_2(\text{high})$ ,  $A_1(\text{LO})$  and  $2A_1(\text{LO})$  phonon mode. Visible emission band may be attributed to both oxygen vacancy and surface states of the thin films. The maximum and minimum band gaps have been found in the thin films grown at 95 and 175 °C, respectively. The fast UV photoresponse is attributed to the adsorption and photodesorption of oxygen molecules on the surface of ZnO thin films. The slow photoresponse may be due to the interactions between oxygen gas and native deep defects.

**Acknowledgments** This work was supported by National Natural Science Foundation of China (Nos. 51472003, 51272001, 51102072, 21201052), Natural Science Foundation of Anhui Higher Education Institution of China (Nos. KJ2012Z336, KJ2013A224), Funds for “136” Talent of Hefei Normal University (No. 2014136KJB03).

## References

1. W.K. Hong, J.I. Sohn, D.-K. Hwang, S.-S. Kwon, G. Jo, S. Song, S.-M. Kim, H.-J. Ko, S.-J. Park, M.E. Welland, T. Lee, *Nano Lett.* **8**, 950–956 (2008)
2. Y.C. Ho, P.Y. Ho, H.C. Lee, S.K. Chang, Y.R. Hong, C.F. Lin, *Sol. Energy Mater. Sol. Cells* **132**, 570–577 (2015)
3. Z. Wang, X. Zhan, Y. Wang, S. Muhammad, Y. Huang, J. He, *Nanoscale* **4**, 2678–2684 (2012)
4. G.N. Panin, H.D. Cho, S.W. Lee, T.W. Kang, *J. Korean Phys. Soc.* **64**, 1403–1406 (2014)
5. H.K. Liang, S.F. Yu, H.Y. Yang, *Appl. Phys. Lett.*, **96** (2010)
6. M.Y. Chuang, H.C. Yu, Y.K. Su, C.H. Hsiao, T.H. Kao, C.S. Huang, Y.C. Huang, J.J. Tsai, S.L. Wu, *Sens. Actuators B-Chem.* **202**, 810–819 (2014)
7. D.K. Kim, C.B. Park, *J. Mater. Sci.-Mater. Electron.* **25**, 5416–5421 (2014)
8. M.E. Fragala, G. Malandrino, M.M. Giangregorio, M. Losurdo, G. Bruno, S. Lettieri, L.S. Amato, P. Maddalena, *Chem. Vap. Depos.* **15**, 327–333 (2009)
9. R. Ayouchi, L. Bentes, C. Casteleiro, O. Conde, C.P. Marques, E. Alves, A.M.C. Moutinho, H.P. Marques, O. Teodoro, R. Schwarz, *Appl. Surf. Sci.* **255**, 5917–5921 (2009)
10. M.A.M. Sarjidan, N.S. Salleh, S.H. Basri, R. Razali, N.K. Za'aba, W.H. Abd Majid, *Mater. Express* **4**, 422–428 (2014)
11. S. Kim, M.S. Kim, G. Nam, J.-Y. Leem, *Electron. Mater. Lett.* **8**, 445–450 (2012)
12. S. Lemlikchi, S. Abdelli-Messaci, S. Lafane, T. Kerdja, A. Guittoum, M. Saad, *Appl. Surf. Sci.* **256**, 5650–5655 (2010)
13. A.G. Milekhin, N.A. Yeryukov, L.L. Sveshnikova, T.A. Duda, C. Himcinschi, E.I. Zenkevich, D.R.T. Zahn, *Appl. Phys. A* **107**, 275–278 (2012)
14. S.K. Panda, C. Jacob, *Appl. Phys. A* **96**, 805–811 (2009)
15. J.M. Jang, C.R. Kim, H. Ryu, M. Razeghi, W.-G. Jung, *J. Alloy. Compd.* **463**, 503–510 (2008)
16. J.H. Yang, J.H. Zheng, H.J. Zhai, L.L. Yang, Y.J. Zhang, J.H. Lang, M. Gao, *J. Alloys Compd.* **475**, 741–744 (2009)
17. B. Ling, Y. Wang, X.W. Sun, Z.L. Dong, N.X. Yang, *IEEE J. Sel. Top. Quantum Electron.* **17**, 801–807 (2011)
18. H. Zhai, J. Zheng, J. Yang, Y. Liu, M. Gao, *Cryst. Res. Technol.* **45**, 647–650 (2010)
19. H. Zhang, L. Shen, S. Guo, *J. Phys. Chem. C* **111**, 12939–12943 (2007)

20. K. Mahmood, S.B. Park, H.J. Sung, *J. Mater. Chem. C* **1**, 3138–3149 (2013)
21. L.W. Wang, F. Wu, D.X. Tian, W.J. Li, L. Fang, C.Y. Kong, M. Zhou, *J. Alloys Compd.* **623**, 367–373 (2015)
22. W.T. Yen, Y.C. Lin, P.C. Yao, J.H. Ke, Y.L. Chen, *Thin Solid Films* **518**, 3882–3885 (2010)
23. R. Ahumada-Lazo, L.M. Torres-Martínez, M.A. Ruíz-Gómez, O.E. Vega-Becerra, M.Z. Figueroa-Torres, *Appl. Surf. Sci.* **322**, 35–40 (2014)
24. J. Xie, X. Meng, Z. Zhou, P. Li, L. Yao, L. Bian, X. Gao, Y. Wei, *Mater. Lett.* **110**, 57–60 (2013)
25. J.J. Lai, Y.J. Lin, Y.H. Chen, H.C. Chang, C.J. Liu, Y.Y. Zou, Y.T. Shih, M.C. Wang, *J. Appl. Phys.* **110**, 013704 (2011)
26. M. Gabás, P. Díaz-Carrasco, F. Agulló-Rueda, P. Herrero, A.R. Landa-Cánovas, J.R. Ramos-Barrado, *Sol. Energy Mater. Sol. Cells* **95**, 2327–2334 (2011)
27. C.Y. Kao, C.L. Hsin, C.W. Huang, S.Y. Yu, C.W. Wang, P.H. Yeh, W.W. Wu, *Nanoscale* **4**, 1476–1480 (2012)
28. A. Bera, D. Basak, *Appl. Phys. Lett.* **94**, 163119 (2009)
29. Y. He, W. Zhang, S. Zhang, X. Kang, W. Peng, Y. Xu, *Sens. Actuators A:Phys.* **181**, 6–12 (2012)